

Photoluminescence and structural studies on extended defect evolution during high-temperature processing of ion-implanted epitaxial silicon

P. K. Giri^{a)}

Materials Science Division, Indira Gandhi Centre for Atomic Research, Kalpakkam 603102, India

S. Coffa, V. Raineri, and V. Privitera

CNR-IMTEEM, Stradale Primosole 50, 95121 Catania, Italy

G. Galvagno, A. La Ferla, and E. Rimini

INFN and Dipartimento di Fisica, Università di Catania, Corso Italia 57, 95129 Catania, Italy

(Received 30 June 2000; accepted for publication 31 January 2001)

Low-temperature photoluminescence (PL) spectroscopy, in conjunction with transmission electron microscopy (TEM) and optical microscopy (OM) have been carried out to investigate the origin of radiative recombination from various extended defects that evolve during high-temperature processing of ion-implanted epitaxial silicon. From PL studies on N₂-annealed samples, we provide spectroscopic evidence of precipitation of the implanted impurities well below the solid-solubility limit. This result is being supported by observations from secondary ion mass spectrometry and spreading resistance profiling of the implanted ions. Cross sectional TEM analyses on these samples reveal <111>-oriented precipitates located in a region containing a high dislocation density. Postimplantation annealing in oxygen ambient results in the formation of dislocations and oxidation-induced stacking faults (OISF). A systematic analysis of PL spectra on different-implanted and preannealed samples, in conjunction with TEM and OM analyses, reveals that the conventionally observed dislocation-related D1 and D2 lines in the PL spectrum is not a characteristic of the OISF, but of the dislocations only. It is shown that the OISF acts as a nonradiative channel for luminescence in silicon. Various other sources of nonradiative channels in silicon are also presented and the efficacy of photoluminescence technique in the characterization of process-induced defects in silicon is discussed. © 2001 American Institute of Physics.

[DOI: 10.1063/1.1357464]

I. INTRODUCTION

With the advent of new materials and advanced processing tools, steered by the stringent technological demands, there is an upsurge of interest in understanding the process-induced defects in semiconductors. In integrated device technology, all the commonly adopted dopants (such as B, P, As, and Sb) are introduced by ion implantation for several advantages that this technique offers. However, the implantation of energetic ions into semiconductors creates lattice defects that can have a dramatic influence on optical and electrical properties of the material. The formation and annealing kinetics of various point defects have been extensively studied for silicon. However, a thorough understanding of various processes of secondary defect formation resulting from postimplantation processing such as rapid thermal annealing (RTA), multistep annealing, and thermal quenching is lacking in the literature.¹⁻⁵ In particular, the mechanism of impurity precipitation, outdiffusion, segregation, and low electrical activation of dopants in epitaxially grown pure silicon with very low impurity content is less

studied.⁶ Defects induced by high-fluence ion implantation and subsequent annealing usually show complex evolution of defects depending on the details of the processing steps.³ For example, thermal history has been shown to play an important role in the evolution of process-induced defects in silicon. A high cooling rate of the crystalline ingot was shown to result in high density of defects.⁷ High temperature annealing is usually performed on implanted silicon to repair lattice damage and it enables electrical activation of dopants. However, such processing gives rise to various secondary defects, of which, dislocations, stacking faults and impurity precipitates have drawn wide attention in the past due to their interference in device performance. Furthermore, for deep diffusion of dopants in Si, very high temperature annealing is utilized. However, such thermal treatment is known to introduce surface defects specific to crystallographic orientation and the type of impurity present in the crystal.⁸ A coherent understanding of the optical and structural properties of these process-induced defects is essential in order to make a potential use of defect engineering with extended defects in silicon-based optoelectronic and microelectronic devices.

Photoluminescence (PL) spectroscopy has been an indispensable tool in the study of optically active defects in silicon, for more than four decades.⁹ PL has been most success-

^{a)} Author to whom correspondence should be addressed; also at Dipartimento di Fisica, Università di Catania, Corso Italia 57, 95129 Catania, Italy; Electronic mail: pkgiri@igcar.ernet.in

fully used in studies of bound-exciton spectra of various impurities in the crystalline Si, which gives rise to the characteristic sharp PL spectra. However, relatively little is known about the luminescence properties of the defects created by ion damage and subsequent annealing, which often give rise to broad featureless PL spectra.^{10,11} There have been few attempts to identify dopant or impurity precipitates in silicon from PL studies,^{11,12} while no definite peak assignments could be made from the previous studies due to lack of complementary techniques. Recently, ion beam synthesized β -FeSi₂ precipitates in Si were found to exhibit the 1.54 μm PL.¹³

Numerous studies have reported the formation of extended defects such as dislocation and stacking faults in ion-implanted Si during thermal oxidation as a result of injection of self-interstitials.¹⁴ The origin of the dislocation-related PL bands (commonly referred to as D lines) in silicon has been the subject of many detailed investigations.¹⁵ However, there exists controversy in the literature about the exact origin of several well known D-lines in PL spectrum, commonly related to dislocations and stacking faults in Si. For example, Peaker *et al.*¹⁶ reported the occurrence of D1 and D2 lines in clean oxidation-induced stacking faults (OISF), while no D lines were observed by Higgs *et al.*¹⁷ in OISF, grown under clean conditions. It is generally believed that the dislocations decorated with impurities give rise to the well known D1 and D2 lines in PL spectrum and the same is believed about OISF from studies on their optical and electronic properties.^{18,19} Hence, more systematic studies on the PL from dislocations and OISF are required to resolve such controversy.

In this work, we have investigated the radiative recombination properties of various extended defects that evolve during high temperature annealing of ion-implanted epitaxial silicon. We use photoluminescence (PL) spectroscopy, transmission electron microscopy (TEM), and optical microscopy (OM) techniques to assess the nature of the defects and their characteristic luminescence properties, which are correlated to their structural properties. In the nitrogen annealed samples, we provide a spectroscopic evidence of impurity precipitation occurring for impurity concentrations well below the solid solubility limit. Studies on OISF and dislocations using complementary techniques, provide evidence that the OISF acts as a nonradiative channel in the luminescence of silicon, while isolated dislocations give rise to characteristic D lines in PL spectrum. Different sources of extended defects and their radiative properties are discussed for thermally processed wafers.

II. EXPERIMENTAL DETAILS

The experiments were performed on phosphorous doped epitaxial (Epi) silicon layers of 60 μm thickness ($\rho \sim 70 \Omega\text{cm}$) grown on floating zone Si wafers. Different ions (Al⁺, B⁺, P⁺, and Si⁺) were implanted on the epitaxial Si layers at an energy of 80 keV and to a fluence of $1 \times 10^{14} \text{cm}^{-2}$ using a 400 kV implanter (High Voltage Engineering). The implanted samples were oxidized with dry O₂ for 1 h at

1200 °C on preannealed or as-implanted wafers. The preannealing was performed in N₂ ambient using RTA for 30 s and 2 min, or furnace annealing for 1 h at a temperature of 1200 °C. 2 min RTA process was performed in four steps of 30 s each with an interval of a few minutes in between for cooling. For furnace annealing, the samples were inserted sufficiently fast in the tube of the horizontal furnace maintained at 1200 °C and taken out at the end of 1 h, without allowing any extra time for slow heating or cooling. The PL measurements were carried out at 16 K using a closed cycle He cryostat, and the luminescence was excited using Ar⁺ laser tuned to 488 nm. The luminescence was analyzed using a CVI spectrometer with a single-grating monochromator and a liquid-nitrogen cooled Ge diode detector (North Coast) was used with a lock-in technique to record the signal. Before performing PL measurements, all oxidized specimens were etched in a buffer hydrofluoric acid solution to remove the surface oxide layers. For OM studies, the oxidized wafers were at first etched in buffer HF solution to remove the oxide layer and subsequently etched for 30 s in Schimmel solution.²⁰ In some cases, longer duration etching was performed for observing the Epi-stacking faults. The extended defects and precipitates were also analyzed by cross sectional transmission electron microscopy (XTEM). The processed samples were mechanically polished to 30 μm and subsequently ion milled at room temperature with 4 keV argon ions. A JEOL 2010 TEM operating at 200 kV was used for recording the image. The chemical profile of the implanted ions was determined by secondary ion mass spectrometry (SIMS) with a 15 keV O₂⁺ primary beam. The rastered area was $250 \times 250 \mu\text{m}^2$ and the diameter of the analyzed area was 60 μm . The electrically active fraction of the implanted Al was determined by spreading resistance profiling (SRP), using a SSM 150 instrument.

III. RESULTS AND DISCUSSION

A. Impurity precipitation during N₂ annealing

Figure 1 shows a typical set of PL spectra recorded at 16 K for Al⁺-implanted Si after postimplantation processing. The spectrum (a) in Fig. 1 shown with dotted line is for virgin silicon wafer, prior to any implantation or processing and it displays several well known luminescence lines related to intrinsic bound exciton transitions labeled as TO+G, TO, and TA.²¹ As-implanted Si shows a broad PL spectrum [marked (b)] in the range 0.73–0.93 eV and two relatively sharp peaks at 997 (I₁) and 1018 meV (W). The broad featureless peak is due to optical centers created by lattice damage and it is found to be independent of the implanted species. Conventionally observed other sharp peaks are absent in the spectra due to low impurity content in the Epi-Si. The sharp line at 1018 meV is related to an intrinsic defect in silicon and is commonly known as W center.²² There is a controversy regarding the exact identification of this defect, as reports exist in favor of models involving vacancy type complex²³ as well as interstitial type defects.^{22,24} However, our studies on depth profile and low-temperature annealing behavior of this defect are strongly suggestive of a small

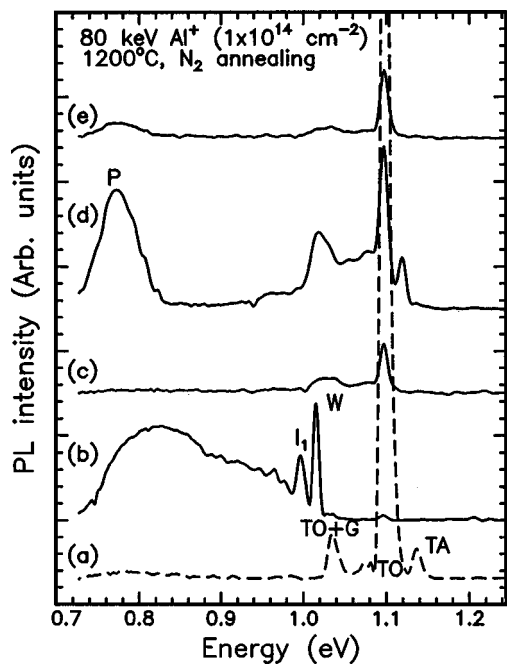


FIG. 1. PL spectra recorded at 16 K for (a) virgin Epi-Si, (b) as-implanted with Al^+ ions, (c) after RTA 30 s, (d) after RTA 2 min, (e) after 1 h furnace annealing in N_2 ambient. Spectra for virgin Si is plotted with dashed line to enable comparison after implantation and annealing.

cluster of self-interstitials. The other peak at 997 meV in Fig. 1 is found to be a phonon replica of the W line. Both these lines disappear after annealing above 450°C for 1 h and we have recently shown that W center is a tri-interstitial cluster of silicon.²⁵

A comparison of spectra in Figs. 1(b), 1(c), and 1(d) shows that with increasing duration of annealing, the TO-phonon related peak recovers to some extent due to gradual recovery of the lattice damage. The spectrum for RTA 2 min annealed sample shows a well formed broad peak (P) at ~ 0.77 eV with a full width at half maximum (FWHM) of ~ 52 meV. Amplitude of this peak reduces substantially after annealing for 1 h as shown in Fig. 1(e). In the RTA 30 s annealed sample, a small increase in the TO-phonon related signal compared to as-implanted sample indicates partial annealing of damage in RTA annealed sample. However, the disappearance of the other features in lower energy part of the spectrum may be attributed to the nonradiative centers introduced in Si during RTA process, as has been noted in the literature.²⁶ The absence of the peak P in Fig. 1(c) also denotes that RTA of 30 s duration is insufficient to create the defect responsible for broad peak at ~ 0.77 eV.

The occurrence of broad PL spectra is often related to the presence of macrodefects such as defect clusters in the crystalline matrix.²⁷ While the nature of the defects responsible for such broad band (BB) PL is not clearly established in the literature, it is well known that various broad PL bands can be present in the bulk silicon after electron irradiation, ion implantation, or reactive-ion etching.²⁸ To isolate the origin of the broad peak P in Fig. 1(d), we have studied PL spectra from different implanted and similarly processed samples. Figure 2 shows the PL spectra for Si samples implanted with Al^+ , B^+ , P^+ , and Si^+ ions with identical flu-

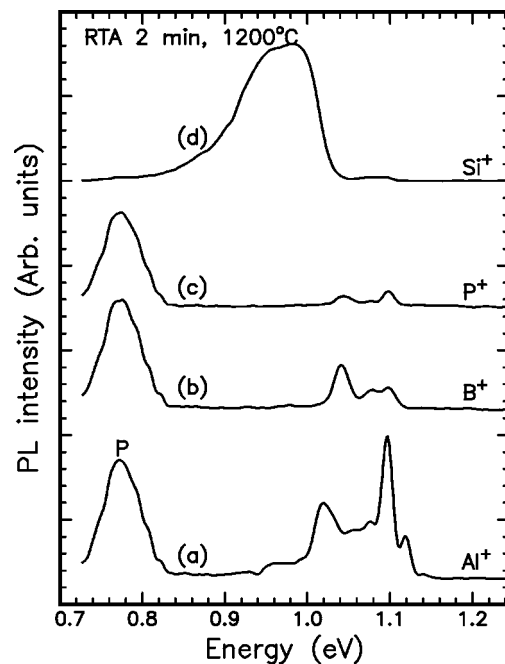


FIG. 2. PL spectra of Si implanted with 80 keV, 1×10^{14} ions/ cm^2 of (a) Al^+ , (b) B^+ , (c) P^+ , and (d) Si^+ , and subsequently 2 min RTA processed at 1200°C in N_2 ambient, showing precipitate-related broad peak (P) at ~ 0.77 eV for all dopant implants.

ence (1×10^{14} cm^{-2}) and RTA processed for 2 min at 1200°C . The peak labeled P at ~ 0.77 eV is common to all dopant implants, while Si^+ -implanted samples show a broader peak at higher energy, as seen in curve (d) of Fig. 2. The occurrence of the broad peak P (at ~ 0.77 eV) with identical line shape and intensity for all the dopant implants indicates a common source of luminescence. The observed P line does not match with any of the D lines related to dislocations. However, this peak was not observed for self-ion-implanted samples. A relatively broader peak with mean position at ~ 0.97 eV can be observed with self-implanted Si as shown in spectrum of Fig. 2(d).

Note that the implanted impurity ions give rise to a peak concentration, which are well below the solid solubility limit of different species used. For example, the 80 keV Al^+ implantation at a fluence of 1×10^{14} cm^{-2} in Si gives rise to a peak concentration of 3.7×10^{18} cm^{-3} as shown in Fig. 3, measured by SIMS analysis. Figure 3 also shows the Al profile after 1 h annealing at 1200°C which exhibits a sharp peak coincident with the implanted Al profile, though a large fraction ($\sim 65\%$) of the implanted Al outdiffuses and another fraction diffuses beyond the projected range owing to its extremely high diffusivity.²⁹ However, spreading resistance profiling of the annealed samples showed that the Al in the peak region is not electrically active (see the dotted line in Fig. 3). This indicates that the Al is precipitated in the annealed sample having a peak concentration of $\sim 1.6 \times 10^{18}$ cm^{-3} at the mean projected range. From Fig. 3, it is seen that beyond a depth of ~ 2.5 μm from surface, all the Al are electrically activated giving rise to a p-type conductivity and a n - p junction is formed at a depth of ~ 5.3 μm from the surface. However, at the present annealing temperature

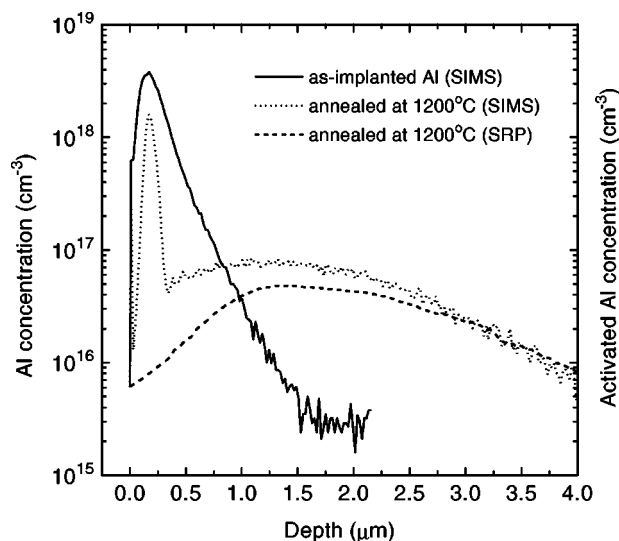


FIG. 3. SIMS profile of the implanted Al in Si before and after annealing at 1200 °C. In the annealed sample, electrically active fraction of the implanted Al is shown with dotted line for comparison with SIMS profile, implying precipitation at the peak location.

(1200 °C), the solubility limit for Al in Si is $2 \times 10^{19} \text{ cm}^{-3}$. For B and P implants, the solubility limit is even much higher than the maximum concentration of implanted ions. Therefore, precipitation of impurities in the present case appears to be unusual.

The solid solubility limit for impurities is well documented in the literature for silicon. However, it applies to thermal-equilibrium conditions that are not always fulfilled under several processes, viz., processes involving high ramping rate of temperatures. In the present case, since the peak P was found to evolve after 2 min RTA, it is believed to result from the defects formed due to the dynamics of damage annealing and the redistribution of the implanted dopants. Note that the absence of the broad peak in the 30 s RTA sample can be related to partial annealing of the damage and insufficient diffusion of impurities to form required precipitates for PL to occur. We believe that the implanted dopants form precipitates in the damaged region during RTA as a result of fast diffusion in the damaged layer and trapping at the extended defects grown during the first stages of annealing. Note that the 2 min RTA was performed in four steps of 30 s each. Dopant precipitation ahead of the moving amorphous/crystalline interface during epitaxial crystallization has been reported to occur as a result of higher diffusivity of the dopants in amorphous Si.³⁰ Therefore, the formation of precipitates in the damaged layer, even at concentrations below the solubility limit is most likely caused by the fast diffusion of implanted impurities and trapping at the damage/crystalline interface. These precipitates are expected to disperse for longer duration annealing. Figure 3 shows that the residual concentration of precipitated Al in annealed samples is sufficient to cause the observed PL signal. It should be noted that due to high thermal nonequilibrium condition created during processes involving high ramp up and ramp down of temperatures, precipitation of impurities is favored. In particular, in the presence of defect-

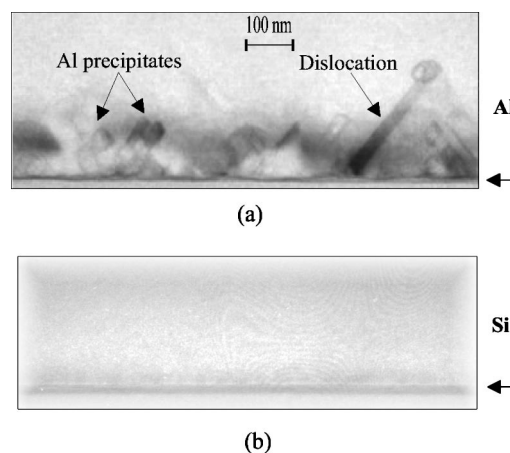


FIG. 4. Bright field cross sectional TEM images taken at 200 kV for different implanted and 2 min RTA annealed Si. (a) Al⁺-implanted Si, showing high density of precipitates and dislocations, and (b) Si⁺-implanted Si showing no defects. The right arrow points to location of the Si surface.

nucleation sites, a heterogeneous precipitation process is expected to occur even below the solid solubility limit. In a high temperature process involving fast heating and cooling (as used in the present case, both for RTA and furnace annealing), precipitation is likely to occur due to the thermal quenching effect as well.⁷ This idea is supported by the fact that precipitation was found to occur even for 1 h furnace annealing process as evidenced from Fig. 1(e) and Fig. 3. Defect formation due to the use of high heating and cooling rate in conventional furnace has been reported to occur in virgin silicon.³¹ Therefore, we believe that both mechanisms, viz., the trapping at extended defects and thermal quenching effect, contribute to the formation of precipitates even for concentrations below the solubility limit of different dopant implants. The broad PL peak P results from strain surrounding these precipitates.

On the other hand, self-ion implantation gives rise to excess silicon interstitials and the extended interstitial chains may form during annealing for a high fluence. The interstitial diffusivity in Si is known to be very high even at room temperature which is consistent with their fast migration and extended defect formation. However, the RTA produces a distribution of these defects such that they experience an inhomogeneous environment and this is believed to result in a relatively broad peak. For higher-temperature annealing, a chain of these defects may align to produce the {311} defects which occur primarily due to the clustering of the interstitials.³² It is most likely that the broad peak in self-ion-implanted Si is due to small chains of interstitials which are not detectable with TEM. We have observed that this BB peak in the spectra appears with low intensity (not shown) for 1 h annealed samples.

The structure of the defects in these RTA annealed samples was further investigated by cross sectional TEM analysis. Figure 4 shows a bright-field XTEM image of Al⁺- and Si⁺-implanted Si after RTA (2 min) annealing. For the Al⁺-implanted sample, the presence of a band of precipitates near the surface region is clearly identified which are pointed with arrows. The precipitate sizes are in the range of

~10–25 nm. It is interesting to note that these precipitates are nucleated at the dislocations, clearly visible with elongated lines [in Fig. 4(a)] oriented along $\langle 111 \rangle$ direction. This may indicate that Al trapping in dislocations is responsible for efficient precipitation,³³ even below solubility limit. Thus, a heterogeneous precipitation can indeed occur even below solid solubility limit. The observed Al precipitates were found to be oriented along $\{111\}$ planes which is consistent with the reported results.³⁴ These precipitates are present both at the end-of-range as well as in the region of ion damage. Note that in spite of the presence of dislocations in these samples, no D lines could be detected in the PL spectra of Fig. 2. It might indicate that the presence of precipitates acts as a nonradiative channel for D-line luminescence. For other dopant implants such as P^+ , similar structure of precipitates are found, but with relatively lower density of dislocations. However, implantation with self-ions does not yield any detectable concentration of dislocations. This difference can be explained in the following way. Self-ion implantation produces excess interstitials, and in the absence of impurity trapping, majority of the interstitials recombines with vacancies, resulting in a faster recovery of the damage during annealing, and thus a reduced density of extended defects. In contrast, implanted dopants (e.g., Al) may form complex with ion-induced defects and during postimplant annealing such complexes dissociate and release defects necessary for the formation of extended defects. In case of Si implants, the size of the chains/clusters may be very small to be detectable by conventional TEM analysis. The occurrence of a higher energy peak (closer to TO phonon-related peak in crystalline Si) in PL than that of impurity precipitates, signifies that the residual damage and stress is very low with self-ion implants. Therefore, observations from PL and TEM analysis are fully consistent.

Dopant precipitation phenomena have been observed during RTA processing of arsenic-implanted Si^{35} or during lamp annealing of antimony-implanted Si.¹² PL studies on oxygen precipitated or antimony precipitated Si also showed similar broad peak.^{11,12} In all these cases, it has been observed for impurity concentrations above the solid solubility limit. In the present case, the origin of broad PL signal can be explained on the basis of a recently proposed model which takes into account the effect of local strain fields surrounding the extended defects such as precipitates, platelets etc., where electrons and holes can be localized in potential wells. It was estimated by Weman and co-workers²⁸ that a compressive strain field around the extended defects, reducing the lattice constant by about 3% is sufficient to reduce the band gap locally by as much as 0.3 eV. In the present case, the precipitated region is highly strained and there exists a size distribution that results in a broad peak in the PL spectrum. The measured FWHM for the spectrum of Fig. 1(d) is 52 meV. This linewidth is expected to decrease for higher temperature RTA processes due to the formation of more uniform precipitates. However, annealing for 1 h reduces the density of such precipitates as seen by the presence of a weak PL signal. To make an estimate of the local strain around these precipitates from the measured peak position of BB, the peak at ~ 0.77 eV which refers to a change in the

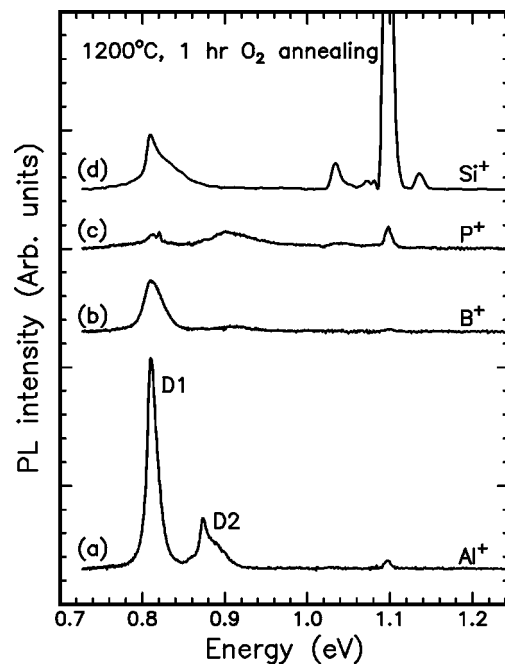


FIG. 5. PL spectra of different ion-implanted and oxygen-annealed Si: (a) Al^+ , (b) B^+ , (c) P^+ , and (d) Si^+ ions. D1 and D2 refers to commonly denoted dislocation related D lines (at 0.810 eV and 0.875 eV, respectively). Surface oxide layer on Si was etched before the PL measurements.

local bandgap of ~ 0.4 eV, would correspond to a strain value ($\Delta a_{\perp}/a_0$) of $\sim 3\%$ according to the model of Ref. 28. A similar BB peak at 0.78 eV has been observed by Buyanova and co-workers²⁷ in p-type modulation doped Si layer grown by molecular beam epitaxy (MBE) where ion damage was involved.

B. Oxidation induced stacking faults and dislocation related photoluminescence

Figure 5 shows a set of PL spectra for Si samples implanted with different ions and subsequently annealed in dry O_2 for 1 h. In case of Al^+ -implanted Si, the spectrum is dominated by a sharp peak at 0.810 eV (labeled D1) and another relatively weak peak at 0.875 eV (labeled D2). The peak at 0.810 eV is common to all spectra in varying intensity, due to different implant species. The peak at 0.810 eV is due to the well-known dislocation-related D1 line, and the peak at 0.875 eV is ascribed to the dislocation-related D2 line.¹⁵ In case of Si^+ implants, D1 line is relatively broader with a higher energy shoulder and the TO phonon related peak (at ~ 1.12 eV) attains very high value comparable to that of virgin Si. This latter feature in Si^+ -implanted samples indicates that sufficient damage recovery or annealing of nonradiative channels occurs during annealing in oxygen ambient. It may be caused by the annihilation of excess vacancies in Si due to the injection of self-interstitials during oxidation. PL studies on preannealed (in N_2 ambient) and oxidized samples show a complete suppression of D lines as well as TO phonon-related signal, in spite of the presence of dislocations and OISF in low concentration. This indicates that defects induced during preannealing act as a nonradiative channel to PL in Si.

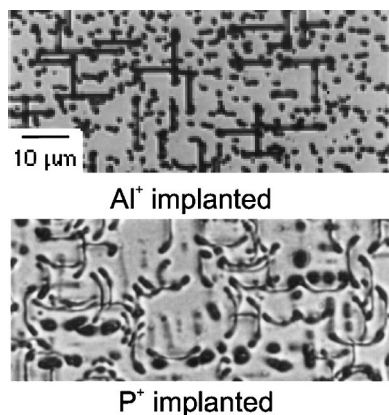


FIG. 6. OM images of oxidized-Si implanted with (a) Al^+ and (b) P^+ , without any preannealing, showing high density of dislocations (dots) and OISF (rod like).

Dislocation related D1 and D2 lines have been extensively studied in literature and is believed to result from bound-to-bound transitions.¹⁵ D1 and D2 lines have been reported to occur in ion-implanted Si, heat-treated Czochralski (CZ) Si, etc. During the oxidation of silicon, a large concentration of silicon interstitials is injected in the silicon matrix at the Si-SiO₂ interface due to change in volume ratio of Si and SiO₂.¹⁴ The lattice damage induced by implantation acts as a nucleation site for the formation of extended defects such as dislocations and stacking faults during oxidation of Si. A relatively strong D1 line in Al^+ -implanted and oxidized silicon indicates that the formation of dislocations and stacking faults were enhanced in case of Al compared to other dopants such as B or P. A comparative study of the optical micrographs shown in Fig. 6 reveals a high density of dislocations and OISF in Al^+ -implanted sample, while it shows Epi-stacking faults for P^+ -implanted sample. Therefore, the absence of D line in P^+ -implanted case is due to the presence of stacking faults and the strong D line in PL spectrum of Al^+ -implanted sample refers to the fact that D1 line originates from the dislocations, not from stacking faults. Furthermore, TEM analysis on P^+ -implanted and oxidized Si does not show any detectable density of dislocations, while optical microscopy shows Epi-stacking faults for P^+ -implanted Si. Therefore, it can be concluded that D1 and D2 lines originate from dislocations, only. On the other hand, OISF acts as a nonradiative channel in the luminescence of silicon, contrary to the belief that OISF exhibits similar D-line luminescence. This is perhaps related to the fact that experimentally it is difficult to form OISFs without the presence of isolated dislocations, as one structure is the basis for the other. Moreover, the stacking fault lines are usually bounded by dislocations at two ends. Thus, the presence of D1 line in PL spectra is commonly related to OISF rather than dislocations, when both of them are present in oxidized Si.¹⁹ However, our results unambiguously show that OISF is a nonradiative center in silicon luminescence.

To clarify further the origin of D1 and D2 lines in this case, in Fig. 7 we compare the results of preannealing on PL, XTEM and OM data. Figure 7(a) shows PL spectra for

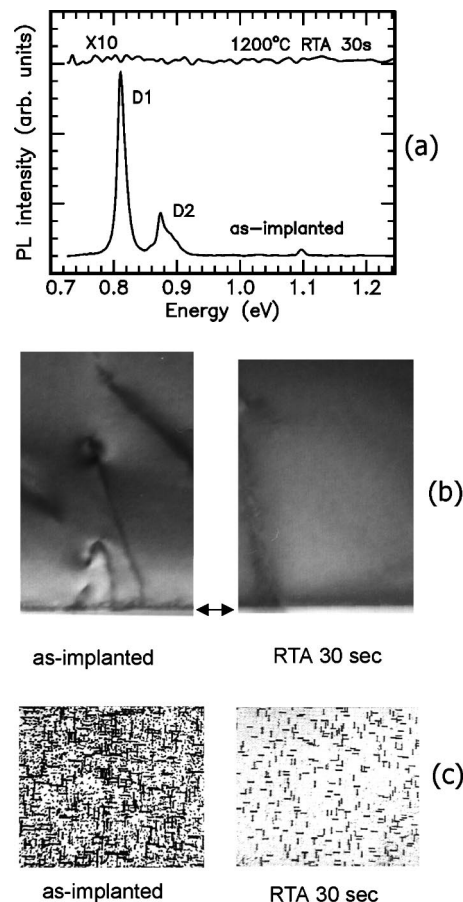


FIG. 7. Comparison of (a) PL spectra, (b) XTEM images, and (c) OM images (magnification $\times 200$), showing the effect of preannealing (1200 °C, RTA 30 s) before oxidation, on extended defect formation in Al^+ -implanted Si.

Al^+ -implanted samples oxidized for 1 h at 1200 °C, without any preannealing or with preannealing (RTA 30 s in N₂ ambient). It is clear that while D1 and D2 lines are identifiable in a sample without the preannealing, no D1 and D2 signal could be detected in the preannealed sample. Note that the upper curve in Fig. 7(a) is shown magnified (10 \times), but does not show any detectable signal, including the TO phonon related peak. Fig. 7(b) shows XTEM image of the above two samples. Al^+ -implanted samples oxidized without preannealing, show high density of dislocations, while preannealed samples show negligible dislocations. This observation again affirms that D1 and D2 lines are directly related to dislocations. This idea is further complemented by OM studies on the above two samples, as shown in Fig. 7(c). It is evident that the OISF densities are approximately equal ($\sim 1.5 \times 10^6 \text{ cm}^{-2}$) in both the cases, while the dislocation density is negligibly small in preannealed sample. This clearly establishes that OISF acts as a nonradiative channel in photoluminescence of silicon. It is believed that decoration of impurity in dislocation is necessary for observing D1 and D2 lines. The presence of D lines in Si⁺-implanted samples implies that the unavoidable contamination in the high-temperature processing (such as from furnace tube) is sufficient to detect D-lines luminescence from dislocations.

TABLE I. Effect of N_2 preannealing on the density and length of OISF and the density of dislocations in oxidized Epi-Si implanted with Al^+ ions.

Preannealing (N_2) before oxidation	Density of OISF (cm^{-2})	Length of OISF (μm)	Density of dislocations (cm^{-2})
No	1.5×10^6	12	10.5×10^6
RTA 30 s	7×10^5	8	$< 10^4$
RTA 2 min	2×10^5	12	$< 10^4$
Furnace 1 h	1×10^5	12	$< 10^4$

In Table I we summarize the results on the optical microscopy observations of OISF density, OISF length, and dislocation density with different preannealing before oxidation. The results indicate that nucleation sites for the OISF growth reduces considerably (orders of magnitude) due to preannealing in N_2 ambient. However, the residual defects act as a nonradiative channel for PL and the TO phonon related peak, affected by these defects. Preannealing for 1 h before oxidation of Si^+ -implanted Si, leads to the survival of sufficient dislocations in comparison to OISF as seen by OM. We correspondingly observe D1 line in PL spectrum for 1 h preannealed Si^+ -implanted sample, but not for other implants. This again strengthens the argument that D1 line is not related to OISF, but rather intrinsically connected to dislocations.

Both the dislocations and the OISF give rise to deep electronic levels in the band gap of Si. In particular, the density of states for OISF has a broad distribution in comparison to the discrete levels introduced by dislocation.^{18,36} The absence of well-defined levels in case of OISF may be responsible for the lack of features in PL spectra. The defect levels induced by dislocations and stacking faults are known to act as a carrier recombination center affecting the electrical properties severely and these deep lying levels are usually nonradiative in nature. Hence, the nonradiative nature of the OISF is consistent with their electronic properties. We observed a relatively strong D1 signal in case of Al implants compared to other dopants. D2 line intensity is negligibly small in case of all implants except for Al. This indicates an enhanced defect formation in Al^+ -implanted silicon. This may be due to the fast diffusion of the Al in silicon and formation of defect-impurity complexes.

C. Other sources of nonradiative channels in annealed silicon

In order to make a comparative study on the role of annealing ambient in defect introduction in virgin silicon, virgin Si samples were annealed in either oxygen or preannealed in nitrogen and subsequently annealed under oxygen ambient. This enables us to isolate the sources of radiative and nonradiative channels in silicon. Figure 8 shows a PL spectra for virgin sample and annealed samples treated under different ambient gases. From spectra in Figs. 8(a) and 8(b), it is clear that oxidation at $1200^\circ C$ does not introduce any nonradiative channel in silicon. On the other hand, when the samples are preannealed in nitrogen ambient for different duration and subsequently oxidized, various nonradiative defects are introduced and they are responsible for the low

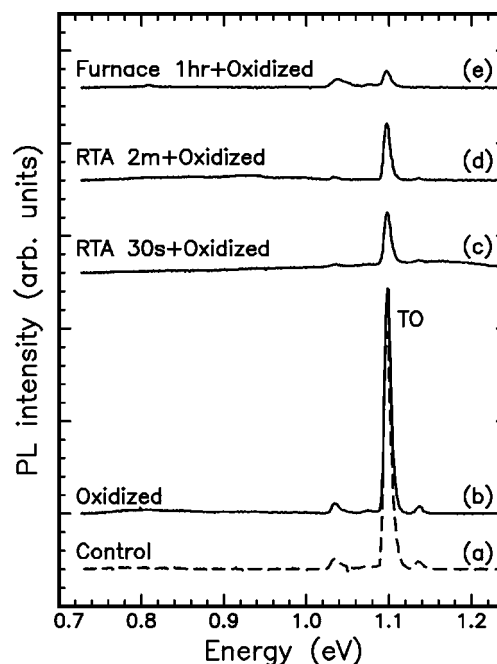


FIG. 8. Effect of annealing ambient on the PL spectra from virgin Epi-Si. (a) Virgin Si, (b) oxygen annealed at $1200^\circ C$ for 1 h (oxidation), (c) RTA 30 s followed by oxidation, (d) RTA 2 min followed by oxidation, and (e) 1 h furnace annealing followed by oxidation. Preannealing in N_2 ambient in each case is shown to introduce nonradiative channels in Si.

intensity of TO phonon line as shown in spectra of Figs. 8(c), 8(d), and 8(e). This implies that high temperature annealing in N_2 introduces nonradiative defects in silicon. In fact, PL measurements on N_2 annealed virgin Si without the oxidation treatment, showed complete absence of TO phonon signals, irrespective of the duration of the annealing. It is to be noted that the N_2 annealing was performed with high ramping of temperature. We believe that thermal stress and unavoidable contamination from furnace tube are likely to be responsible for introducing nonradiative channels in silicon. Defects introduced by RTA process are known to reduce the carrier lifetime in silicon and these defects have been usually related with the impurities in the crystal.³⁷ From OM studies on preannealed and oxidized unimplanted silicon, we found a small but detectable concentration of stacking faults, which may be related to unavoidable contamination by impurities. Furthermore, it is well known that the oxidation of Si causes injection of self-interstitials,¹⁴ whereas high-temperature nitrogen annealing is likely to inject vacancies in the bulk silicon. It is well established that the bulk silicon contains excess vacancies at thermal equilibrium.³⁸ During oxidation, injected interstitials can easily recombine with the vacancies leading to reduced vacancy concentration in silicon. However, during nitridation, injected vacancies are likely to form bigger clusters of vacancies in the bulk due to the absence of interstitials. However, the stable vacancy clusters have been predicted to be optically inactive.³⁹ These vacancy clusters may be responsible for the reduced peak height in PL signal.⁴⁰ Hence, vacancy type defects are likely to be nonradiative channels for silicon to suppress PL in silicon.⁴¹

III. CONCLUSIONS

The radiative recombination at various extended defects that evolve during high temperature processing of ion-implanted silicon has been studied by PL spectroscopy and the results are correlated with the structural properties of the defects. We have shown that annealing in N₂ ambient gives rise to defects that are distinctly different from those that form during annealing in O₂ ambient. We have provided spectroscopic evidence of dopant precipitation during rapid thermal annealing of implanted Epi-Si, for dopant concentration well below the solid solubility limit. The precipitation is believed to result from the fast diffusion of dopants in the damaged region and the corresponding trapping by extended defects as a result of high ramp-rate process. XTEM analysis on these samples shows that these precipitates were oriented along $\langle 111 \rangle$ direction and they are located in a region containing dislocations. These dislocations are believed to assist the precipitation process by trapping of impurities. Annealing of the implanted silicon in O₂ ambient results in the formation of dislocations and OISF. A strong PL signal for dislocation related D1 and D2 lines in Al⁺-implanted samples indicates enhanced defect formation with Al compared to other dopants. A combined use of PL, XTEM, and OM technique for oxidized silicon reveals that D1 and D2 lines in PL spectrum are not characteristic of OISF as is commonly believed, but primarily of dislocations. It is shown that OISF rather acts as a nonradiative channel in silicon photoluminescence. These studies demonstrate the suitability of PL technique in understanding extended-defect evolution during high-temperature processing of silicon.

ACKNOWLEDGMENTS

The authors would like to thank A. Gasparotto (Università di Padova, Italy) for the SIMS measurements. They are grateful to F. Priolo, A. Marino, M. Furnari, and S. Panniteri for their expert technical assistance in sample preparation. This work was partially supported by ICTP, Trieste, under TRIL fellowship program.

¹W. M. Bullis, *Mater. Sci. Eng.*, B **71**, 276 (2000).

²R. Tian, *Nucl. Instrum. Methods Phys. Res. B* **160**, 355 (2000).

³K. S. Jones, S. Prussin, and E. R. Weber, *Appl. Phys. A* **45**, 1 (1988).

⁴M. Tamura, N. Natsuaki, Y. Wada, and E. Mitani, *J. Appl. Phys.* **59**, 3417 (1986).

⁵A. Claverie, L. F. Giles, M. Omri, B. de Mauduit, G. Ben Assayag, and D. Mathiot, *Nucl. Instrum. Methods Phys. Res. B* **147**, 1 (1999).

⁶K. Sumino, *Mater. Sci. Eng.*, B **72**, 67 (2000).

⁷G. Kissinger, D. Graf, U. Lambert, T. Grabolla, and H. Richter, *Semicond. Sci. Technol.* **12**, 933 (1997).

⁸D. Barge, J. P. Jolly, G. Rolland, and B. Pichaud, *Mater. Sci. Eng.*, B **71**, 276 (2000).

⁹G. Davies, *Phys. Rep.* **176**, 83 (1989).

¹⁰N. Magnea, A. Lazrak, and J. L. Pautrat, *Appl. Phys. Lett.* **45**, 60 (1984).

¹¹H. Weman, B. Monemar, and P. O. Holtz, *Appl. Phys. Lett.* **47**, 1110 (1984).

¹²J. Wagner, J. C. Gelpey, and R. T. Hodgson, *Appl. Phys. Lett.* **45**, 47 (1984).

¹³C. Spinella, S. Coffa, C. Bongiorno, S. Panniteri, and M. G. Grimaldi, *Appl. Phys. Lett.* **76**, 173 (2000).

¹⁴S. M. Hu, *Mater. Sci. Eng.*, R **13**, 105 (1994).

¹⁵R. Sauer, J. Weber, J. Stolz, E. R. Weber, K.-H. Kusters, and H. Alexander, *Appl. Phys. A* **36**, 1 (1985), and references therein.

¹⁶A. R. Peaker, B. Hamilton, G. R. Lahiji, I. E. Ture, and G. Lorimer, *Mater. Sci. Eng.*, B **4**, 123 (1989).

¹⁷V. Higgs, M. Goulding, A. Brinklow, and P. Kightley, *Appl. Phys. Lett.* **60**, 1369 (1989).

¹⁸M. Saritas and A. R. Peaker, *Solid-State Electron.* **38**, 1025 (1995).

¹⁹J. H. Evans, J. Kaniewski, M. Kaniewska, and J. S. Rimmer, *Semicond. Sci. Technol.* **7**, A41 (1992).

²⁰D. G. Schimmel, *J. Electrochem. Soc.* **126**, 479 (1979).

²¹P. J. Dean, J. R. Haynes, and W. F. Flood, *Phys. Rev.* **161**, 711 (1967).

²²P. J. Schultz, T. D. Thomson, and R. G. Elliman, *Appl. Phys. Lett.* **60**, 59 (1992).

²³S. K. Estreicher, J. Weber, A. Derecskei-Kovacs, and D. S. Marynick, *Phys. Rev. B* **55**, 5037 (1997).

²⁴G. Davies, E. C. Lightowers, and Z. E. Ciechanowska, *J. Phys.: Condens. Matter* **20**, 191 (1997); H. Feick and E. R. Weber, *Physica B* **273**, 497 (1999).

²⁵P. K. Giri, S. Coffa, and F. Rimini, *Appl. Phys. Lett.* (in press).

²⁶N.-E. Chabane-Sari, L. Thibaud, S. Kaddour, M. Berenguer, and D. Barbier, *J. Appl. Phys.* **71**, 3320 (1992).

²⁷I. A. Buyanova, W. M. Chen, A. Henry, W. X. Ni, G. V. Hanson, and B. Monemar, *Phys. Rev. B* **52**, 12006 (1995), and references therein.

²⁸H. Weman, B. Monemar, G. S. Oehrlein, and S. J. Jeng, *Phys. Rev. B* **42**, 3109 (1990).

²⁹G. Galvagno, F. La Via, F. Priolo, and E. Rimini, *Semicond. Sci. Technol.* **8**, 488 (1993).

³⁰J. Narayan, O. W. Holland, and B. R. Appleton, *J. Vac. Sci. Technol. B* **1**, 871 (1983).

³¹S. Prussin, *J. Appl. Phys.* **43**, 733 (1972).

³²N. Arai, S. Takeda, and M. Kohyama, *Phys. Rev. Lett.* **78**, 4265 (1997).

³³C. Ortiz, J. J. Grob, D. Mathiot, A. Claverie, C. Dubois, and R. Jerisian, *Nucl. Instrum. Methods Phys. Res. B* **147**, 122 (1999).

³⁴D. K. Sadana, M. H. Norcott, R. G. Wilson, and U. Dahmen, *Appl. Phys. Lett.* **49**, 1169 (1986).

³⁵O. W. Holland, J. Narayan, D. Fathey, and S. R. Wilson, *Appl. Phys. Lett.* **59**, 905 (1986).

³⁶P. Omling, E. R. Weber, L. Montelius, H. Alexander, and J. Michel, *Phys. Rev. B* **32**, 6571 (1985).

³⁷Y. Tokuda, N. Kobayashi, A. Usami, Y. Inoue, and M. Imura, *J. Appl. Phys.* **66**, 3651 (1989).

³⁸T. Okino and T. Shimozaki, *Physica B* **273**, 509 (1999).

³⁹S. K. Estreicher, J. L. Hastings, and P. A. Fedders, *Appl. Phys. Lett.* **70**, 432 (1997).

⁴⁰D. A. Redman, D. M. Follstaedt, T. R. Guilinger, and M. J. Kelly, *Appl. Phys. Lett.* **65**, 2386 (1994).

⁴¹R. Siegel, G. C. Weatherly, H. K. Haugen, D. J. Dickwood, and L. M. Howe, *Appl. Phys. Lett.* **66**, 1319 (1995).